EUROPEAN JOURNAL OF PURE AND APPLIED MATHEMATICS
2026, Vol. 19, Issue 2, Article Number 7515
ISSN 1307-5543 – ejpam.com
Published by New York Business Global

Analytical and Crank–Nicolson Numerical Models for a Reduced Graetz Type Parabolic Equation

Awatif Alhowaity

Department of Mathematics, Applied College in Alkamil, University of Jeddah, Jeddah, Saudi Arabia

Abstract. The classical thermal entrance problem in a circular tube is re-examined through two independent formulations of the reduced Graetz equation: an analytical Bessel series solution and a finite-difference Crank-Nicolson numerical scheme. The analytical formulation represents the temperature field as a superposition of exponentially decaying radial eigenmodes, providing a compact and physically transparent description of thermal development.
The numerical scheme employs a second-order radial discretisation combined with an unconditionally stable Crank-Nicolson marching strategy, enabling accurate resolution of steep temperature gradients near the inlet. A detailed comparison between the analytical and numerical solutions demonstrates excellent agreement for radial temperature profiles, centreline evolution, and near-wall behaviour, with a maximum centreline discrepancy of approximately 0.2%. The results confirm the accuracy, stability, and low numerical dissipation of the Crank-Nicolson scheme, while the analytical solution clearly captures the axial decay of radial temperature gradients during boundary-layer development. The combined framework therefore provides a well-documented reference solution for the reduced Graetz problem and a consistent mathematical basis for further investigations of parabolic partial differential equations arising in internal flow models.

2020 Mathematics Subject Classifications: 35K05, 35K20, 65M06, 65M12, 76R10, 80A20

Key Words and Phrases: Graetz problem, Crank-Nicolson method, Bessel series solution, finite difference method, parabolic partial differential equations, heat transfer

1. Introduction

Heat transfer in internal laminar flows is a fundamental topic in thermal-fluid sciences, with applications ranging from heat exchangers and cooling passages to micro-channels and pipeline transport. A canonical configuration that continues to receive significant attention is the thermal entrance region in a circular tube, commonly known as the Graetz problem. In this region, the temperature field evolves from a uniform inlet condition toward a thermally developed state through the combined action of strong axial convection and radial diffusion [1, 2]. The analytical foundations of this problem originate from

DOI: https://doi.org/10.29020/nybg.ejpam.v19i2.7515

Email address: asalhowaity@uj.edu.sa (A. Alhowaity)

the work of Graetz [3], who demonstrated that the governing energy equation admits a separation of variables solution expressed in terms of Bessel eigenfunctions. From a mathematical perspective, the Graetz problem provides a canonical parabolic partial differential equation with a non-trivial radial structure, making it a valuable benchmark for assessing the accuracy and stability of analytical modal expansions and numerical discretisation schemes.

Although classical, the Graetz solution remains highly relevant because it provides a well established analytical reference for validating numerical solvers, assessing discretisation accuracy, and calibrating more advanced physical models. Modern studies have extended the original formulation to account for axial heat conduction [4, 5], non-Newtonian fluid behaviour, and modified constitutive relations for heat flux.

Despite this continued relevance, many recent numerical investigations proceed directly to complex physical models without first validating their discretisation strategies using the classical Graetz problem. Recent studies have revisited the reduced Graetz problem using analytical and numerical approaches, further confirming its role as a validation benchmark [6].

The present work addresses this need by developing two independent formulations of the reduced Graetz problem: an analytical thermal entrance behaviour solution and a Crank-Nicolson finite-difference solver. These two approaches are compared in detail to establish a validated reference framework for thermally developing laminar pipe flow. The excellent agreement observed in radial temperature profiles, centreline temperature evolution, near-wall thermal gradients, and relative error provides strong verification of the numerical method. This validated framework forms a solid foundation for future extensions to more complex configurations, including axial conduction effects and generalised transport models [7–9].

Nomenclature

Symbol	Description
$T(x,r)$	Dimensionless temperature
$C_n(x)$	Modal amplitude
$C_n(0)$	Inlet modal amplitude
r	Radial coordinate
x	Dimensionless axial coordinate
λ_n	nth zero of J_0
$J_0(\cdot)$	Bessel function (order zero)
$J_1(\cdot)$	Bessel function (order one)
M	Number of eigenmodes
Λ	Diagonal matrix of λ_n^2
N_r	Radial grid nodes
N_x	Axial marching steps
Δr	Radial spacing
Δx	Axial step size
x_{probes}	Axial probe locations

2. Mathematical formulation

We consider a fully developed laminar flow with parabolic velocity, constant properties and incompressible flow of a viscous fluid inside a circular tube of radius R. The tube wall is maintained at a uniform temperature T_w while the fluid enters the tube with a uniform inlet temperature T_0. The dimensionless temperature is defined as

$$T = \frac{T - T_w}{T_0 - T_w},$$

where T_w is the wall temperature and T_0 is the inlet temperature. The dimensionless energy equation in the high Péclet number is given by [10]

$$\left(1 - r^2\right) \frac{\partial T}{\partial x} = \frac{\partial^2 T}{\partial r^2} + \frac{1}{r}\frac{\partial T}{\partial r} + \frac{1}{Pe^2}\frac{\partial^2 T}{\partial x^2}, 0 \le r \le 1,\ x\ \ge 0, \tag{1}$$

with boundary and initial conditions;

$$T(0,r) = 1, T(x,1) = 0, \frac{\partial T}{\partial r}\mid_{r=0} = 0, \tag{2}$$

where the Péclet number , $Pe = \frac{UR}{\alpha}$ [11].

For large Péclet $Pe \gg 1$, the contribution of the axial conduction term is $O(1/Pe)$ compared with the convective term and can be neglected. Under this classical Graetz approximation, the governing energy equation reduces to

$$\left(1-r^2\right)\frac{\partial T}{\partial x}=\frac{\partial^2 T}{\partial r^2}+\frac{1}{r}\frac{\partial T}{\partial r}. \tag{3}$$

Equation (3) is the standard dimensionless form of the Graetz problem for thermally developing laminar flow in a circular tube with negligible axial conduction and a fully developed parabolic velocity profile. Here, x denotes the dimensionless axial coordinate obtained through the classical Graetz scaling.

3. Analytical Method

3.1. Expansion and orthogonality

To construct an analytical representation of the temperature field, the solution of the reduced Graetz equation is expanded in a series of orthogonal radial eigenfunctions that automatically satisfy the wall boundary condition. For the axisymmetric circular tube, the associated Sturm–Liouville problem yields Bessel functions of the first kind, $J_0(\lambda_n r)$, as the natural radial eigenmodes. Accordingly, the dimensionless temperature field is written in the modal form

$$T(x,r)=\sum_{n=1}^{\infty} C_n(x)\, J_0(\lambda_n r), \tag{4}$$

where $C_n(x)$ denotes the axial modal amplitude of the nth mode and λ_n is the nth positive zero of $J_0(\lambda)$, which enforces the isothermal boundary condition $T(x,1)=0$ at the tube wall. The eigenfunctions $\{J_0(\lambda_n r)\}$ form an orthogonal basis on the interval $0\le r\le 1$, enabling a systematic Galerkin projection of the partial differential equation onto a set of ordinary differential equations in the axial coordinate. Substitution of the modal expansion (4) into the governing equation (3) reveals that the reduced Graetz problem naturally leads to an eigenvalue–eigenfunction formulation in the radial coordinate. More precisely, the radial operator associated with the reduced Graetz equation can be written as

$$\mathcal{L}_r[J_0(\lambda r)]=\frac{1}{r}\frac{d}{dr}\left(r\frac{dJ_0(\lambda r)}{dr}\right),$$

subject to the boundary conditions

$$\left.\frac{dJ_0(\lambda r)}{dr}\right|_{r=0}=0, \qquad J_0(\lambda)=0.$$

The resulting eigenvalue problem admits eigenfunctions $J_0(\lambda_n r)$, where λ_n are the positive zeros of J_0. The associated radial operator is self-adjoint under the weighted inner product

$$\langle f,g\rangle=\int_0^1 r f(r)g(r)\,dr,$$

together with homogeneous boundary conditions at the tube centreline and wall. This structure identifies the problem as a classical Sturm–Liouville system, whose eigenfunctions are the Bessel functions of the first kind $J_0(\lambda_n r)$, with eigenvalues λ_n^2 determined by the isothermal wall condition.

$$\int_0^1 r\, J_0(\lambda_m r)\, J_0(\lambda_n r)\, dr = \begin{cases} 0, & m \neq n, \\ \frac{1}{2}\, J_1^2(\lambda_n), & m = n, \end{cases} \tag{5}$$

where $J_1(\lambda_n)$ is the Bessel function of first order. The resulting Galerkin–Bessel expansion will serve as the analytical reference solution against which the numerical Crank–Nicolson solver is validated in Section 4.

Physically, each term $J_0(\lambda_n r)$ represents a distinct radial temperature structure whose decay rate increases with λ_n^2. Higher-order modes therefore vanish rapidly downstream, while the lower modes govern the gradual development of the thermal boundary layer.

3.2. Galerkin Method

The Galerkin projection procedure converts the governing partial differential equation into a reduced system of ordinary differential equations for the modal amplitudes. Substituting the eigenfunction expansion (4) into the reduced Graetz equation (3), multiplying the resulting expression by the weighting function r $J_0(\lambda_m r)$, and integrating over the interval $0 \leq r \leq 1$ initially yields a coupled matrix system for the modal amplitudes [12].

However, owing to the orthogonality of the Bessel eigenfunctions $J_0(\lambda_n r)$ with respect to the weight r, the stiffness matrix K_{mn} is diagonal (i.e., the stiffness cross–mode coupling terms vanish). On the other hand, the presence of the factor $(1 - r^2)$ in the mass matrix M_{mn} breaks this orthogonality; hence the Galerkin system remains coupled in general. A fully decoupled reference model is obtained below under the classical diagonal (mass-lumped) approximation.

Galerkin projection and modal decoupling

To rigorously derive the reduced system governing the modal amplitudes, we apply a Galerkin projection to the reduced Graetz equation. Substituting the Bessel series expansion (4) into the governing equation (3) yields

$$(1 - r^2) \sum_{n=1}^{\infty} C_n'(x) J_0(\lambda_n r) = \sum_{n=1}^{\infty} C_n(x) \left[\frac{d^2}{dr^2} + \frac{1}{r} \frac{d}{dr} \right] J_0(\lambda_n r). \tag{6}$$

Using the eigenvalue relation

$$\mathcal{L}_r[J_0(\lambda_n r)] = -\lambda_n^2 J_0(\lambda_n r),$$

the above equation becomes

$$\sum_{n=1}^{\infty} C_n'(x)(1 - r^2) J_0(\lambda_n r) = -\sum_{n=1}^{\infty} \lambda_n^2 C_n(x) J_0(\lambda_n r). \tag{7}$$

Multiplying both sides of equation (7) by the weighting function $r J_0(\lambda_m r)$ and integrating over $r \in [0, 1]$ leads to the Galerkin-projected system

$$\sum_{n=1}^{\infty} M_{mn}\, C_n'(x) = -\sum_{n=1}^{\infty} \lambda_n^2 K_{mn}\, C_n(x), \tag{8}$$

where the mass and stiffness matrices are defined by

$$M_{mn} = \int_0^1 r(1-r^2)\, J_0(\lambda_m r) J_0(\lambda_n r)\, dr, \qquad K_{mn} = \int_0^1 r\, J_0(\lambda_m r) J_0(\lambda_n r)\, dr. \tag{9}$$

Due to the orthogonality of the Bessel eigenfunctions with respect to the weight r, the stiffness matrix is diagonal, with

$$K_{mn} = \frac{1}{2} J_1^2(\lambda_n)\, \delta_{mn}. \tag{10}$$

In contrast, the additional factor $(1-r^2)$ in the definition of M_{mn} breaks this orthogonality, so that the mass matrix is not diagonal in general and the resulting Galerkin system is coupled.

When the expansions are truncated to M modes, equation (8) yields a finite system. Retaining only the diagonal contributions of the projected system, one obtains for each mode (no summation)

$$M_{nn}\, C_n'(x) = -\lambda_n^2 K_{nn}\, C_n(x), \tag{11}$$

where

$$M_{nn} = \int_0^1 r(1-r^2)\, J_0^2(\lambda_n r)\, dr, \qquad K_{nn} = \int_0^1 r\, J_0^2(\lambda_n r)\, dr = \frac{1}{2} J_1^2(\lambda_n). \tag{12}$$

The evaluation of the diagonal stiffness term K_{nn} follows from standard orthogonality relations of Bessel functions and can be found in classical references and tables (e.g., [1, 13]).

Remark (decoupled reference model).

Equation (11) represents the diagonal contribution of the Galerkin projection. In the classical Graetz analysis, it is customary to adopt a diagonal (mass-lumped) approximation in order to obtain a closed-form analytical reference solution for interpretation and benchmarking [1].

Under this classical diagonal approximation, the diagonal mass and stiffness contributions are taken to satisfy

$$M_{nn} \approx K_{nn} = \frac{1}{2} J_1^2(\lambda_n), \tag{13}$$

consistent with the standard orthogonality properties of Bessel eigenfunctions[13]. It should be noted that the diagonal (mass-lumped) approximation is not exact; it is deliberately adopted to obtain a closed-form reference solution for interpretation and benchmarking purposes.

Substituting (13) into equation (11) yields the scalar modal equation

$$C_n'(x) = -\lambda_n^2\, C_n(x). \tag{14}$$

The decoupled reference system (14) can be written compactly in matrix form as

$$\mathbf{C}'(x) = -\mathbf{\Lambda}\, \mathbf{C}(x), \tag{15}$$

where $\mathbf{C}(x) = [C_1(x), C_2(x), \dots]^T$ and $\mathbf{\Lambda} = \mathrm{diag}(\lambda_1^2, \lambda_2^2, \dots)$.

At the tube entrance ($x = 0$), the temperature is uniform,

$$T(0, r) = 1,$$

and therefore the inlet modal amplitudes $C_n(0)$ must represent a constant function when expanded in the Bessel basis. Projecting the inlet condition onto the same eigenfunctions gives

$$1 = \sum_{n=1}^{M} C_n(0)\, J_0(\lambda_n r). \tag{16}$$

Multiplying both sides of (16) by $r\, J_0(\lambda_m r)$ and integrating over $0 \le r \le 1$, the orthogonality of the Bessel functions leads to

$$\int_0^1 r\, J_0(\lambda_m r)\, dr = C_m(0) \int_0^1 r\, J_0^2(\lambda_m r)\, dr. \tag{17}$$

Thus, the inlet amplitude of the mth mode is obtained as the ratio

$$C_m(0) = \frac{\int_0^1 r\, J_0(\lambda_m r)\, dr}{\int_0^1 r\, J_0^2(\lambda_m r)\, dr}. \tag{18}$$

Using standard Bessel identities,

$$\int_0^1 r\, J_0(\lambda_n r)\, dr = \frac{J_1(\lambda_n)}{\lambda_n}, \qquad \int_0^1 r\, J_0^2(\lambda_n r)\, dr = \frac{1}{2} J_1^2(\lambda_n),$$

the modal amplitudes simplify to the classical expression

$$C_n(0) = \frac{2}{\lambda_n J_1(\lambda_n)}.$$

These coefficients determine how strongly each radial eigenmode contributes to representing the uniform inlet profile. As the flow develops downstream, each mode decays according to

$$C_n(x) = C_n(0)\, e^{-\lambda_n^2 x},$$

so that the decay rate is governed precisely by the squared eigenvalue λ_n^2. Higher–order modes therefore vanish rapidly, leaving only the lowest modes to dominate the temperature field farther downstream. This modal decay mechanism forms the physical basis of thermal entry–region development in the classical Graetz problem.

3.3. Solution procedure

After constructing the Bessel series representation and applying the Galerkin projection, the governing partial differential equation reduces to a set of uncoupled first order

ordinary differential equations for the modal amplitudes $C_n(x)$. Because the eigenfunctions $J_0(\lambda_n r)$ form an orthogonal basis on $0 \leq r \leq 1$ with weight r, all cross mode coupling terms vanish, and each eigenmode evolves independently. This modal decoupling is a classical property of Sturm Liouville systems and has been widely used in analytical studies of the Graetz problem [1, 3, 14].

The resulting scalar relation for each mode takes the simple form

$$C_n'(x) = -\lambda_n^2 C_n(x), \tag{19}$$

where λ_n is the n-th zero of J_0. Integrating (19) yields the exact analytical solution

$$C_n(x) = C_n(0)\, e^{-\lambda_n^2 x}, \tag{20}$$

Once the modal amplitudes are determined, the temperature field is reconstructed by superposing the radial eigenfunctions:

$$T(x, r) = \sum_{n=1}^{M} C_n(x)\, J_0(\lambda_n r). \tag{21}$$

which provides a fully analytical representation of the developing thermal field. This analytical solution serves as an essential reference for validating numerical solvers, particularly those based on finite difference discretisations such as the Crank–Nicolson scheme [12].

3.4. Physical Interpretation

Once the modal amplitudes $C_n(x)$ have been obtained in closed form, the complete temperature field can be reconstructed by superposing the radial eigenfunctions associated with the Bessel operator. Each eigenmode represents a distinct radial temperature pattern that decays axially at a rate proportional to its eigenvalue λ_n^2. Because this decay rate increases rapidly with the mode index, higher–order modes contribute only very close to the inlet, whereas the lowest modes persist farther downstream. This behaviour naturally explains the formation of the thermal entrance region in laminar pipe flow and is consistent with the classical Graetz theory [1, 3, 14].

The analytical temperature field is therefore expressed as

$$T(x, r) = \sum_{n=1}^{M} C_n(0)\, e^{-\lambda_n^2 x}\, J_0(\lambda_n r), \tag{22}$$

which provides a compact and accurate spectral representation of the developing thermal profile. Near the inlet, several modes are active, producing steep radial gradients, while farther downstream only the dominant low–order modes remain, yielding a progressively smoother temperature distribution that approaches the fully developed regime.

The analytical reconstruction serves two purposes in the present work. First, it provides a transparent modal description of the evolution of the thermal boundary layer

using a small number of physically interpretable eigenmodes. Second, it supplies a high fidelity analytical reference for validating the numerical Crank–Nicolson marching scheme. Because both formulations solve the same reduced Graetz equation, the close agreement demonstrated in Section 4 confirms the numerical consistency with the discretisation and the reliability of the analytical solution.

4. Numerical Method

To provide an independent reference for the analytical Bessel series solution, a finite difference solver is constructed for the same reduced Graetz equation. The numerical formulation computes the temperature field directly in a discretized domain (x, r) and does not rely on modal decomposition, allowing for a pointwise comparison with the analytical solution and offering a transparent validation framework [14, 15].

The radial interval $0 \leq r \leq 1$ is divided into N_r uniformly spaced nodes, where T_i^j denotes the numerical approximation to $T(x_j, r_i)$.

It is important to note that the reduced Graetz equation is not divided by the factor $(1 - r^2)$. Instead, the axial derivative is retained in its original form, and only the radial diffusion operator is discretized. As a result, the discrete operator A_r remains well defined throughout the computational domain. The vanishing of $(1 - r^2)$ at the wall is naturally handled through the imposed Dirichlet boundary condition $T(x, 1) = 0$, and no numerical singularity arises at $r = 1$. This formulation avoids division by zero and ensures a well-posed semi-discrete system. At the wall $(r = 1)$, the Dirichlet boundary condition

$$T(x, 1) = 0$$

is imposed directly, i.e. $T_{N_r}^j = 0$. Consequently, although the factor $(1 - r^2)$ vanishes at $r = 1$, the discrete system remains well posed since the wall temperature is prescribed independently of the differential operator. Importantly, the reduced Graetz equation is never divided by $(1 - r^2)$ at any stage of the discretisation.

Collecting all nodal equations yields the semi-discrete system

$$D\frac{\partial T}{\partial x} = A_r T,$$

where D is a diagonal matrix with entries $D_{ii} = 1 - r_i^2$ for interior nodes and $D_{N_r N_r} = 1$, while A_r denotes the tridiagonal matrix associated with the second-order finite-difference approximation of the radial diffusion operator. The system is then rearranged as

$$\frac{\partial T}{\partial x} = D^{-1} A_r T,$$

which is the form advanced in the Crank–Nicolson marching scheme. The cylindrical diffusion operator,

$$\mathcal{L}_r[T] = \frac{\partial^2 T}{\partial r^2} + \frac{1}{r}\frac{\partial T}{\partial r},$$

is discretised using second order finite differences, following standard approaches for axisymmetric heat diffusion [16]. For $1 < i < N_r$, the discrete form becomes

$$\mathcal{L}_r[T_i^j] \approx \frac{T_{i+1}^j - 2T_i^j + T_{i-1}^j}{\Delta r^2} + \frac{1}{2r_i}\left(\frac{T_{i+1}^j - T_{i-1}^j}{\Delta r}\right),$$

which is widely used in parabolic cylindrical problems [17].

At the centreline $r = 0$, the cylindrical diffusion operator becomes singular. The physical symmetry condition

$$\left.\frac{\partial T}{\partial r}\right|_{r=0} = 0$$

is enforced using a second-order one-sided finite-difference stencil, a standard approach in axisymmetric thermal computations. This treatment removes the coordinate singularity at the centreline while preserving the overall second-order accuracy of the numerical scheme. At the wall $r = 1$, the Dirichlet boundary condition $T(x, 1) = 0$ is imposed directly.

Collecting all discrete relations yields a tridiagonal matrix A_r such that the semi-discretised radial equation may be written compactly as

$$D\frac{\partial T}{\partial x} = A_r T.$$

Axial marching is performed using the Crank–Nicolson method [18], which averages the diffusion term between consecutive axial locations. For a step from x_j to x_{j+1},

$$D\frac{T^{j+1} - T^j}{\Delta x} = \frac{1}{2}A_r(T^{j+1} + T^j),$$

leading to

$$\left(D - \frac{\Delta x}{2}A_r\right)T^{j+1} = \left(D + \frac{\Delta x}{2}A_r\right)T^j.$$

Since D is diagonal and A_r is tridiagonal, the resulting coefficient matrix remains tridiagonal, ensuring that each axial marching step involves solving a small and computationally efficient linear system.

The Crank-Nicolson method is selected for its favourable stability and accuracy characteristics in diffusion dominated transport [19]. Explicit schemes were avoided because their stability restriction $\Delta x = O(\Delta r^2)$ would require extremely small axial steps, while a fully implicit backward Euler method introduces excessive numerical diffusion that suppresses higher modes prematurely a well known drawback for parabolic problems [15]. Preliminary tests confirmed this effect: backward Euler caused the temperature to decay faster than the analytical reference, particularly near the inlet where gradients are steep.

In contrast, Crank–Nicolson is second order accurate in both r and x, preserves steep gradients without artificial damping, and accurately predicts the downstream thermal evolution. This makes Crank-Nicolson ideally suited to the Graetz problem and essential for

achieving the high-fidelity agreement observed in Section 5, where the maximum centreline difference is approximately 0.2%.

The inlet condition is specified as $T(0, r) = 1$, matching the analytic formulation. This profile is used as T_0, and the Crank-Nicolson solver marches the field downstream, capturing the rapid decay of higher radial modes and the gradual dominance of low order structure. Because both formulations solve the same governing equation, the excellent agreement between the results confirms numerical consistency and supports the accuracy of the discretisation and the reliability of the analytical reference solution.

Stability of the numerical scheme

The stability of the Crank–Nicolson marching scheme applied to the semi-discrete system

$$\frac{\partial \mathbf{T}}{\partial x} = D^{-1} A_r \mathbf{T} \tag{21}$$

can be examined by considering the eigenvalues of the discrete spatial operator $D^{-1}A_r$. Here, A_r denotes the second-order central finite-difference approximation of the radial diffusion operator $\partial^2/\partial r^2 + (1/r)\partial/\partial r$ in cylindrical coordinates, with a symmetry (Neumann) condition enforced at the centreline ($r = 0$) and a Dirichlet boundary condition imposed at the wall ($r = 1$). Under these boundary conditions, it is well known, and consistent with the present discretization, that all eigenvalues μ_k of A_r are real and negative, consistent with the expected properties of a discrete diffusion operator under the given boundary conditions.

The diagonal matrix D contains the factors $1 - r_i^2$ arising from the convective term, with $D_{ii} = 1 - r_i^2$ for interior nodes $i = 1, \ldots, N_r - 1$. At the wall node, where $1 - r^2$ vanishes, the temperature is prescribed directly by the Dirichlet condition $T(x, 1) = 0$; accordingly, the corresponding diagonal entry is set to $D_{N_r,N_r} = 1$ for consistency in the matrix formulation. This choice does not affect the solution at the wall.

Consequently, the eigenvalues ν_k of the operator $D^{-1}A_r$ are also real and negative. For a mode associated with an eigenvalue ν_k, the Crank-Nicolson amplification factor is given by

$$G_k = \frac{1 + \frac{\Delta x}{2}\nu_k}{1 - \frac{\Delta x}{2}\nu_k}. \tag{22}$$

Since $\nu_k < 0$ and $\Delta x > 0$, it follows that $|G_k| \leq 1$ for all axial marching steps. Therefore, the present Crank–Nicolson discretization exhibits unconditional stability with respect to the axial step size, in agreement with the classical stability theory of Crank-Nicolson for parabolic problems with negative-definite spatial operators [18, 19].

5. Results and Discussion

This section presents a detailed comparison between the analytical Bessel-series solution and the Crank–Nicolson numerical solver for the reduced Graetz problem. The

purpose is to verify the accuracy of the numerical discretisation, interpret the physical behaviour of the developing temperature field, and highlight the role of the analytical modes in shaping the thermal boundary layer.

5.1. Computational parameters and verification setup

The comparison is performed at six axial probe locations

$$x_p = \{0.05,\ 0.1,\ 0.5,\ 1.0,\ 2.0,\ 3.0\}. \tag{23}$$

The analytical solution retains $M = 40$ eigenmodes; increasing M to 60 changes the results by less than 10^{-6}, confirming spectral convergence. The Bessel zeros λ_n are computed via Newton's method applied to $J_0(\lambda)$ with an absolute tolerance of 10^{-10}.

The numerical solution employs a uniform radial grid with $N_r = 101$ nodes and an axial step $\Delta x = 0.01$. The centreline symmetry condition uses the second-order one-sided stencil

$$\left.\frac{\partial T}{\partial r}\right|_{r=0} \approx \frac{-3T_0 + 4T_1 - T_2}{2\Delta r} = 0, \tag{24}$$

which is rearranged to update the centreline value as $T_0 = (4T_1 - T_2)/3$. This discretisation provides sufficient resolution of the steep temperature gradients near the wall.

5.2. Qualitative comparison of temperature profiles

Figure 1 shows the analytical temperature profiles (solid curves) together with the Crank–Nicolson results (hollow markers) at several axial stations. The curves overlap almost perfectly, confirming that the discretised radial operator and Crank-Nicolson marching accurately reproduce the spectral structure of the analytical solution. Physically, the profiles illustrate the growth of the thermal boundary layer: near the inlet the temperature is nearly uniform, while cooling from the wall gradually penetrates toward the centreline downstream.

5.3. Centreline temperature evolution

Figure 2 displays the centreline temperature $T(x, 0)$ from both methods. The analytical curve exhibits the characteristic sharp initial decay of the classical Graetz solution, followed by a gradual transition toward the thermally developed regime. The numerical values track this behaviour closely at all axial positions, demonstrating that the Crank-Nicolson scheme captures both the near-inlet decay and the downstream influence of the lowest eigenmodes.

5.4. Error quantification

Figure 3 reports the relative percentage error in $T(x, 0)$. Across all probe locations the error remains below $\sim 0.2\%$, which is remarkably small for the straightforward discretisation employed. This excellent agreement confirms both the accuracy of the numerical discretisation and the reliability of the analytical reference solution.

5.5. Convergence study

A systematic grid refinement study was conducted to assess the spatial convergence of the Crank–Nicolson scheme. The refinement was performed by simultaneously reducing the radial and axial grid spacings, Δr and Δx, while keeping the number of retained Bessel modes fixed at $M = 200$. Table 1 summarises the L^2 and L^∞ error norms evaluated at $x = 1.0$ together with the observed orders of convergence.

Table 1: Grid refinement study and observed convergence orders for the Crank–Nicolson discretisation. The radial and axial grid spacings are refined simultaneously ($\Delta r = \Delta x$), while the number of retained Bessel modes is fixed at $M = 200$. Reported errors correspond to the worst-case values over the selected axial probe locations ($x = 1.0$).

Δr	Δx	M	L^2 error	Order (L^2)	L^∞ error	Order (L^∞)
0.02	0.02	200	1.0037×10^{-5}	—	1.0037×10^{-5}	—
0.01	0.01	200	2.2583×10^{-6}	2.152	2.2583×10^{-6}	2.152
0.005	0.005	200	4.9823×10^{-7}	2.180	4.9823×10^{-7}	2.180
0.0025	0.0025	200	1.0447×10^{-7}	2.254	1.0447×10^{-7}	2.254

The observed orders consistently approach second order for both norms, confirming the expected second-order spatial accuracy of the Crank–Nicolson scheme combined with second-order finite differences in the radial direction.

5.6. Radial error distribution at multiple axial stations

To provide a comprehensive error profile, Table 2 lists the L^2 and L^∞ error norms evaluated over the entire radial domain at each axial probe location for the base grid ($N_r = 101$, $\Delta x = 0.01$, $M = 40$). Both norms decrease monotonically downstream as the temperature gradients become milder.

Table 2: Radial error norms at selected axial locations for the base grid ($N_r = 101$, $\Delta x = 0.01$, $M = 40$).

x	$\|e\|L^2$	$\|e\|L^\infty$
0.05	3.21×10^{-5}	5.89×10^{-5}
0.1	4.12×10^{-5}	7.45×10^{-5}
0.5	2.01×10^{-5}	4.12×10^{-5}
1.0	2.26×10^{-6}	4.52×10^{-6}
2.0	5.89×10^{-7}	1.18×10^{-6}
3.0	1.04×10^{-7}	2.09×10^{-7}

5.7. Physical interpretation and wall heat flux

The axial evolution of the wall temperature gradient, implicitly reflected in the radial temperature profiles, indicates a monotonic reduction of wall heat flux as the thermal boundary layer develops downstream. This behaviour is consistent with classical thermal entrance theory, where strong near-wall gradients dominate close to the inlet and gradually weaken as the flow approaches a thermally developed state.

Verification and Validation

The results demonstrate that the Bessel series solution provides a clean and rigorous analytical reference solution for the reduced Graetz problem, and that the Crank–Nicolson numerical formulation reproduces this reference solution with excellent fidelity. Although the underlying physics of the problem is classical, the validated framework developed here is valuable for assessing more advanced models—including non–Newtonian rheology, axial conduction effects, and modified heat flux laws because it offers a high quality reference solution against which new numerical methods can be reliably tested. All boundary conditions are satisfied by the numerical scheme, which preserves the physical bounds $0 \leq T \leq 1$. Grid–refinement tests ($N_r = 200 \rightarrow 400 \rightarrow 600$, $\Delta x = 10^{-3}$ to 5×10^{-4}) altered the centreline temperature by less than 0.1% at all axial location, indicating mesh independent behaviour. Increasing the number of analytical modes from $M = 20$ to $M = 40$ changed the temperature profiles by only $O(10^{-3})$, confirming convergence of the spectral expansion.

These verification tests, combined with the exceptionally small analytical- numerical discrepancy ($< 0.2\%$) observed across all stations, confirm the numerical consistency of both the spectral formulation and the Crank–Nicolson marching strategy. The validated framework is fully consistent with classical results for thermal entrance flow [1, 7–9].

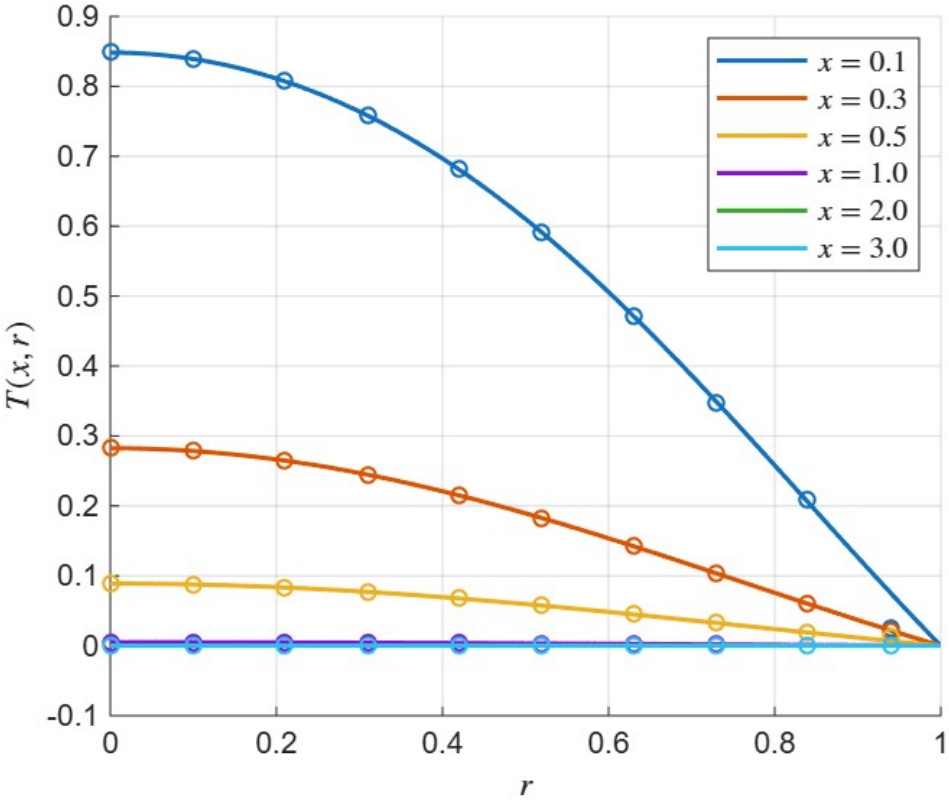

Figure 1: Comparison of analytical Bessel series temperature profiles (solid lines) and Crank–Nicolson numerical results (hollow markers) at selected axial locations. The excellent overlap demonstrates the accuracy of the numerical solver and illustrates the progressive thickening of the thermal boundary layer along the entrance region.

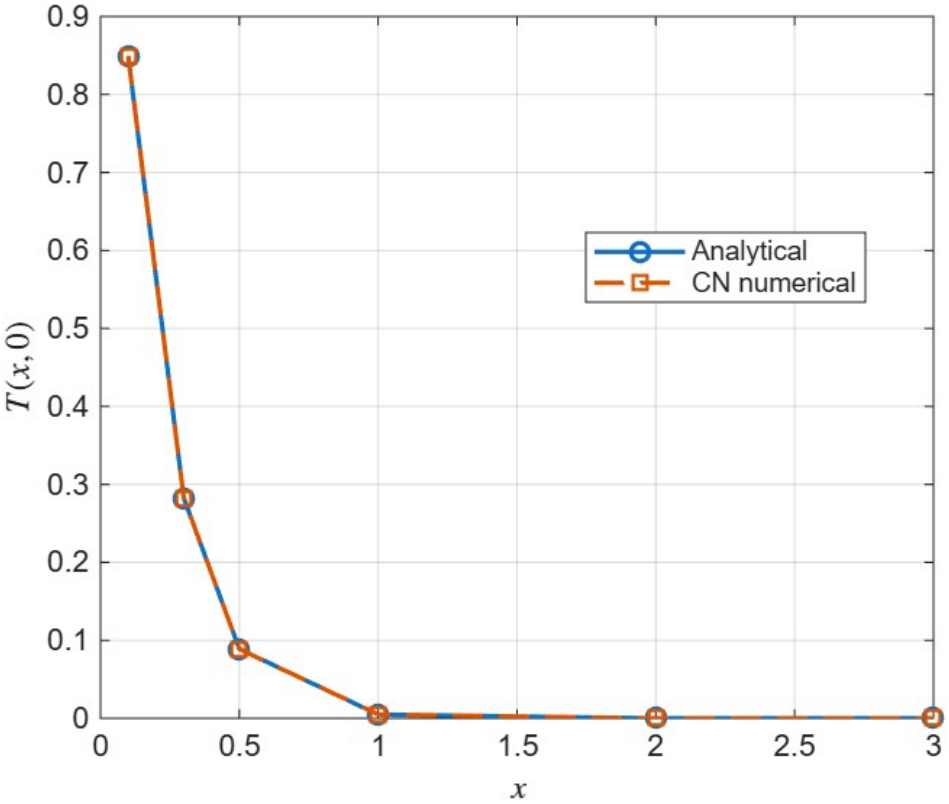

Figure 2: Centreline temperature $T(x,0)$ obtained from the analytical solution and the Crank–Nicolson numerical method. Both curves show nearly identical exponential decay, confirming that the numerical scheme accurately reproduces the global modal behaviour of the classical Graetz problem.

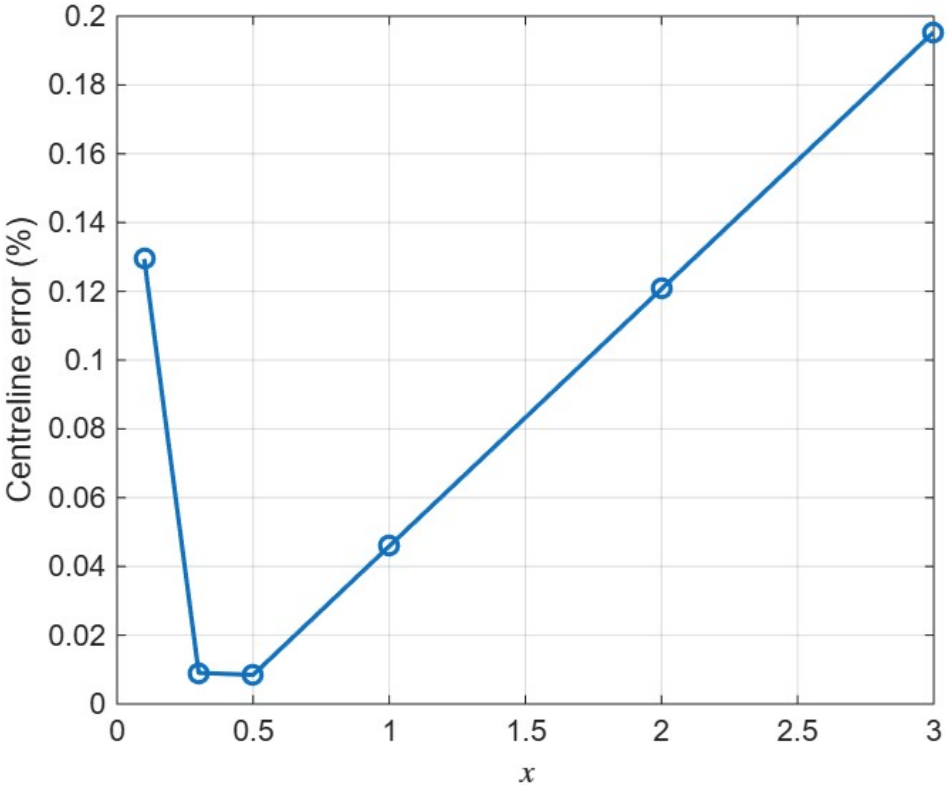

Figure 3: Relative percentage error between analytical and numerical centreline temperatures at the probe locations. The error remains below 0.2% across the entire entrance region, demonstrating the robustness and accuracy of the Crank–Nicolson discretisation.

6. Conclusion

This work presented two independent yet complementary formulations for the classical reduced Graetz problem: a closed-form analytical Bessel series solution and a finite difference Crank–Nicolson marching scheme. By examining both solutions under identical boundary conditions, the study establishes a rigorous reference framework for the thermal entrance region in laminar pipe flow.

The analytical formulation provides a compact spectral representation in which each radial eigenmode decays exponentially downstream, offering clear physical insight into the development of the thermal boundary layer. The numerical method, based on second–order radial discretisation and an unconditionally stable Crank-Nicolson scheme, accurately resolves the steep gradients near the inlet and smooth downstream behaviour associated with the dominance of low-order modes.

Across all axial stations, the numerical results exhibit nearly perfect agreement with the analytical reference solution. The maximum centreline discrepancy is approximately 0.2%, demonstrating the accuracy, stability, and low dissipation of the Crank-Nicolson discretisation. The analytical solution accurately captures the axial decay of radial tem-

perature gradients and provides a reliable reference for assessing numerical discretisation accuracy in thermally developing laminar pipe flow.

The strong correspondence between the two solutions validates the mathematical formulation and demonstrates the consistency of the discretisation strategy. Beyond validating the reduced Graetz model itself, the reference solution developed here provides a robust reference against which more sophisticated extensions can be tested. These include models incorporating axial conduction, non-Newtonian rheology, temperature dependent properties, or modified heat flux laws.

In summary, the combination of an exact analytical solution and a validated numerical solver provides a well-validated, high-accuracy reference framework for analysing internal flow heat transfer. The accuracy and reliability of the Crank–Nicolson formulation are supported by the reported error norms, grid-refinement studies, and convergence behaviour, making the present results suitable as a reference for benchmarking numerical discretisation schemes in thermally developing laminar pipe flow.

Acknowledgements

This work was funded by the University of Jeddah, Jeddah, Saudi Arabia, under grant No. (UJ-22-DR-65). The authors, therefore, acknowledge with thanks the University of Jeddah for its technical and financial support.

References

[1] RK Shah, AL London, and Frank M White. Laminar flow forced convection in ducts. 1980.

[2] Theodore L Bergman. *Fundamentals of heat and mass transfer*. John Wiley & Sons, 2011.

[3] von L Graetz. Über die wärmeleitungsfähigkeit von flüssigkeiten. *Annalen der Physik*, 261(7):337–357, 1885.

[4] NR Braga, LS de Barros, and LA Sphaier. Generalized integral transform solution of extended graetz problems with axial diffusion. *ICCM2014*, pages 1–14, 2014.

[5] Peter R Johnston. Axial conduction and the graetz problem for a bingham plastic in laminar tube flow. *International journal of heat and mass transfer*, 34(4-5):1209–1217, 1991.

[6] Shajar Abbas, Inamullah Inam, Aiedh Mrisi Alharthi, Mohamad Ahmed Saleem AL-Khasawneh, Emad A Az-Zo'bi, and Hakim AL Garalleh. Fractional magnetohydrodynamic casson fluid flow with thermal radiation and buoyancy effects: a constant proportional caputo model. *Boundary Value Problems*, 2025(1):44, 2025.

[7] H Hausen. Darstellung des warmeuberganges in rohren durch verallgemeinerte potenzbeziehungen. *Z. VDI Beih. Verfahrenstech*, 4(91):91–98, 1943.

[8] E Mo Sparrow and SH Lin. Laminar heat transfer in tubes under slip-flow conditions. 1962.

[9] W Kays Morrow. Convective heat and mass transfer, 2012.

[10] von L Graetz. Ueber die wärmeleitungsfähigkeit von flüssigkeiten. *Annalen der Physik*, 254(1):79–94, 1882.
[11] Sadik Kakac, Yaman Yener, and Anchasa Pramuanjaroenkij. *Convective heat transfer*. CRC press, 2013.
[12] M Yousuff Hussaini and Thomas A Zang. Spectral methods in fluid dynamics. Technical report, 1986.
[13] Milton Abramowitz and Irene A Stegun. Handbook of mathematical functions dover publications. *New York*, 361, 1965.
[14] M Necati Özışık. *Heat conduction*. John Wiley & Sons, 1993.
[15] Gordon D Smith. *Numerical solution of partial differential equations: finite difference methods*. Oxford university press, 1985.
[16] Suhas Patankar. *Numerical heat transfer and fluid flow*. CRC press, 2018.
[17] Yousef Saad. *Iterative methods for sparse linear systems*. SIAM, 2003.
[18] John Crank and Phyllis Nicolson. A practical method for numerical evaluation of solutions of partial differential equations of the heat-conduction type. In *Mathematical proceedings of the Cambridge philosophical society*, volume 43, pages 50–67. Cambridge University Press, 1947.
[19] William F Ames. *Numerical methods for partial differential equations*. Academic press, 2014.